








# Parametric Analysis of Journal Bearings with Chevron Textures on the Shaft Surface

Luis F. dos Anjos<sup>1</sup> , Alfredo Jaramillo<sup>2</sup> , Gustavo C. Buscaglia<sup>2</sup> ,  
and Rodrigo Nicoletti<sup>1</sup>  

<sup>1</sup> Sao Carlos School of Engineering, University of Sao Paulo, Sao Carlos, Brazil  
luis.anjos@usp.br, rnicolet@sc.usp.br

<sup>2</sup> Institute of Mathematical Sciences and Computation, University of Sao Paulo, Sao Carlos, Brazil  
gustavo.buscaglia@icmc.usp.br

**Abstract.** Surface texturing has proven to be a good technique to improve the characteristics of lubricated contacts. In journal bearings, texturing can increase the load-carrying capacity and reduce friction between the surfaces depending on some texture parameters such as geometry, size, and position. Although many works are studying the influence of textures on journal bearings, most of them apply the texture on the bearing surface (static part of the contact). In this work, chevron-shaped textures are applied on the shaft surface (moving part of the bearing) and a parametric analysis is performed considering some geometric parameters of the chevron. The fluid flow is modeled using the Reynolds equation and a mass-conserving boundary condition is used to deal with the cavitation zones. Due to the moving nature of the texture (imposed on the rotating surface of the shaft), a moving grid technique is employed in the Finite Volumes scheme. The results show the existence of optimal texture shapes depending on the Sommerfeld number of the bearing (operating condition). The textures with optimum shapes can reduce the shaft eccentricity, which indicates an increase in load-carrying capacity. The reason for this increase in load-carrying capacity is explained by an analysis of the lubricant's flow dynamics in the bearing during operation, where a pumping effect is observed which reduces the leakage flow (the bearing with textured shaft keeps more lubricant in the bearing gap than the plain journal bearing).

**Keywords:** Moving Grid · Finite Volumes Method · Hydrodynamic Lubrication

## 1 Introduction

The increasing demand for more energetically efficient machines led Engineering to seek ways of reducing losses during operation. One of these ways that have been investigated is the texturization of surfaces in sliding and/or lubricated contacts. In this case, texturization can be considered as any imposed alteration of the surface topology, be it of a structured or random nature.

The first studies on the subject focused on the unstructured textures imposed on the surface by conventional machining manufacturing processes [1, 2]. It was observed that

the presence of irregularities on the surface of sliding contacts did improve some hydrodynamic properties due to the pressure build-up and cavitation effects in the region of these irregularities. Hence, there came the idea of purposely imposing such irregularities on the surface of sliding contacts in a more organized (or structured) way, trying to take advantage of the resultant hydrodynamic effects to improve the behavior of the lubricated contact. Such an idea was fostered in the last decades with the advent of modern machining techniques that allowed the controlled imposition of micrometric textures on surfaces within acceptable tolerances: ion etching [3], abrasive jet machining [4, 5], laser surface texturing [5, 6], mechanical micro drawing [7], grinding texturing [8].

In the last decades, much has been investigated on the application of structured textures in lubricated contacts, especially in journal bearings and sliding bearings. Texturized surfaces were studied under different lubricating regimes [9–11], and they resulted in similar reductions in the friction coefficient. It has been assumed that the textures work as lubricant reservoirs and they provide additional lubrication under starved or boundary lubricating regimes. Such an explanation is not consensual among researchers, and the most accepted hypothesis is that textures locally change the hydrodynamic pressure distribution in the contact (pressure build-up) due to the presence of local cavitation regions. As a consequence, one achieves an overall increase in the load-carrying capacity of the contact [12].

In journal bearings, surface texturing can modify important static characteristics, such as the rotor eccentricity, the attitude angle, the driving torque, and the oil flow. In this case, the geometry, size, and position of the textures play an important role to achieve positive results. However, despite the high number of works investigating the subject, there is no consensus in the literature about the best texturing parameters in general terms. For example, the adoption of chevron-type textures in the loaded area of the bearing bush presented good results [13], whereas the adoption of square-type textures in the same region was detrimental in comparison to a full texturized bearing bush [14].

Many different texture geometries have been studied in the literature, including circular [15], rectangular [16], triangular [17], and chevron [18], with all presenting promising results under different operating conditions of the bearing. However, in the majority of the works, the texture is applied to the static surface of the contact. Few works focused on the texturization of the moving parts of the lubricated contact. For example, one observed friction reduction in the sliding contact of a cylinder piston when the surface of the piston had dimple patterns [19]. By adopting grooves on the surface of the cylinder, one observed a bigger retention of lubricant on the sliding surface (an increase of lubricant wetness) [20].

In the case of journal bearings, four different texture geometries were tested experimentally on the surface of the rotating shaft: chevron, sawtooth, oblong dimple, and aligned dimple [21]. In this case, the chevron-type texture significantly decreased the rotor eccentricity in comparison to the non-textured case, as evidenced by the increase in the load-carrying capacity of the bearing. In another work, the sawtooth pattern showed to be a better solution in comparison to the trapezoidal pattern, which is still better than the bearing with a non-textured shaft [22].

The present work focuses on the analysis of a journal bearing supporting a shaft with chevron textures on its surface. The results bring some insight into the physics behind the increase of the load-carrying capacity of the bearing due to the presence of the textures. It is observed that chevron-type textures have a positive pumping effect on the lubricant flow in the bearing gap, thus keeping more fluid in the centerline of the bearing. As a result, the load capacity increases. In addition, the orientation of the chevron pattern plays an important role in the results: if the shaft rotates in the wrong direction, detrimental effects are observed (reduction of load capacity due to pumping of lubricant out of the bearing).

## 2 Mathematical Model

By adopting the classic assumptions for the fluid flow in the lubricated bearing gap, one achieves the Reynolds equation in adimensional form, considering the film fraction in the cavitation zones:

$$\nabla \cdot (h^3 \nabla p) = \alpha \frac{\partial(\theta h)}{\partial x_1} + 2 \frac{\partial(\theta h)}{\partial t} \tag{1}$$

where  $h(x, y, t)$  is the adimensional oil film thickness,  $p(x, y, t)$  is the adimensional oil hydrodynamic pressure,  $\alpha$  is the adimensional shaft velocity,  $t$  is the adimensional time,  $\theta(x, y, t)$  is the oil film fraction, and  $(x, y)$  is a local coordinate system in the planified surface of the bearing ( $x$  in tangential direction and  $y$  in axial direction). When  $\theta = 1$ , there is full film lubrication and  $p \geq 0$ , whereas when  $0 \leq \theta < 1$ , there is cavitation and  $p = 0$ .

The oil film thickness is composed of two terms:

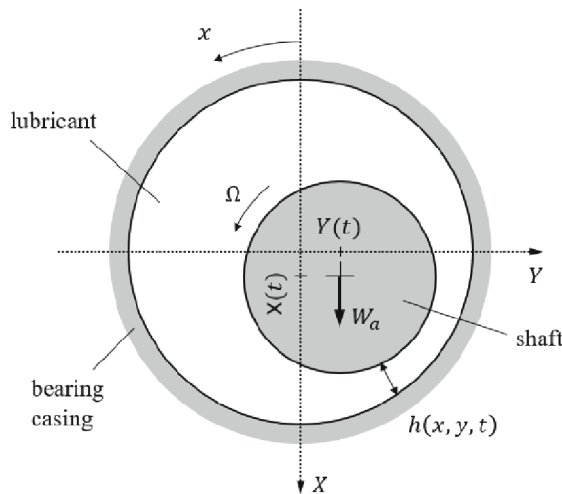


Fig. 1. Global and local coordinate system in the journal bearing.

$$h(x, y, t) = h_f(x, y, t) + h_t(x, y, t) \quad (2)$$

where  $h_f$  is the oil film thickness in the regions without texture, and  $h_t$  is the oil film thickness in the regions with texture. The oil film thickness in the regions without texture ( $h_f$ ) can be written as a function of the position of the shaft in the global coordinate system:

$$h_f(x, y, t) = 1 + X(t) \cos(2\pi x) + Y(t) \sin(2\pi x) \quad (3)$$

where  $X(t)$  and  $Y(t)$  are the coordinated of the center of the shaft in the global coordinate system of the bearing (Fig. 1). To find the position of the shaft, one solves the force equilibrium problem by the Newmark method:

$$\begin{cases} M \frac{d^2 X}{dt^2} = W_X(t) + W_a \\ M \frac{d^2 Y}{dt^2} = W_Y(t) \end{cases} \quad (4)$$

where  $M$  is the shaft mass,  $W_X$  and  $W_Y$  are the components of the hydrodynamic forces in the  $(X, Y)$  global coordinate system, and  $W_a$  is the external loading applied on the shaft.

The second term of Eq. (2) depends on the adopted texture geometry and on the rotating speed of the shaft. For a given instant of time, one has:

$$h_t(x, y, t) = \begin{cases} d & \text{if } (x, y) \in \Gamma \\ 0 & \text{if } (x, y) \notin \Gamma \end{cases} \quad (5)$$

where  $d$  is the texture depth, and  $\Gamma$  is the texture domain. The main challenge in modelling the lubricated contact with textures in the moving surface is the fact that the  $\Gamma$  region moves ( $h_t$  varies with time). To tackle this problem numerically, one moves the domain of the numerical solution  $\Lambda$  (in which Eq. (1) is solved) instead of  $\Gamma$ , thus artificially keeping the texture domain in place. Hence, for every instant of time, the numerical domain moves by  $d\Lambda = \Omega R dt$ , where  $\Omega$  is the shaft rotating speed and  $R$  the shaft radius. Figure 2 shows the motion of the numerical domain  $\Lambda$  in two different instants of time. In a fixed reference frame, the domain  $\Lambda$  moves from left to right. However, in the local reference coordinate system (fixed at the numerical domain  $\Lambda$ ), the texture domain  $\Gamma$  moves from right to the left.

The use of multigrid techniques [23] also proved advantageous to reduce computational costs during the numerical simulations of the system.

### 3 Parametric Analysis

The parameters of the journal bearing in analysis and the operating conditions are listed in Table 1. One considers ambient pressure as the boundary condition for solving the Reynolds equation in the numerical domain  $\Lambda$ :

$$\begin{cases} p(0, y, t) = p(L, y, t) = p_{amb}(\text{supply groove}) \\ p(x, 0, t) = p(x, B, t) = p_{amb}(\text{axial boundary}) \end{cases} \quad (6)$$

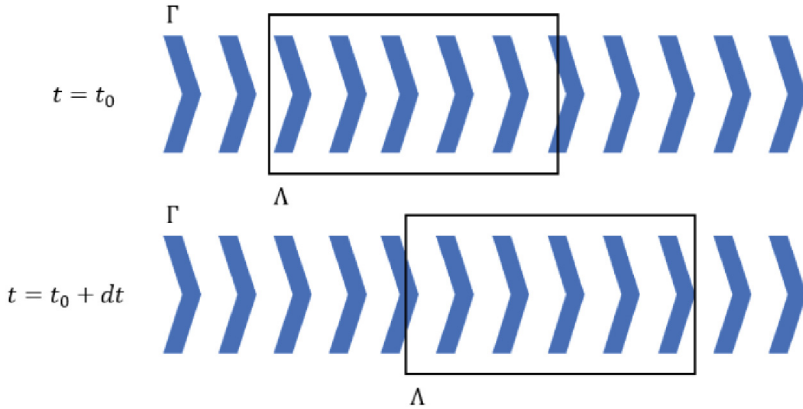


**Fig. 2.** The domain of numerical solution  $\Lambda$  at two different instants of time.

where  $L$  is the total circumferential length of the bearing, and  $B$  is the bearing width. The geometric parameters of the chevron texture are the chevron angle ( $\alpha$ ), the chevron thickness ( $e$ ), and the number of chevrons in the texture ( $N_t$ ) – Fig. 3. The depth of the texture is  $25 \mu\text{m}$  in all studied cases.

**Table 1.** Parameter values of the bearing in analysis.

Parameter	Value	Unit	Parameter	Value	Unit
Bearing width ( $B$ )	25	mm	Rotating speed	4,000	rpm
Bearing nominal clearance ( $h_N$ )	50	$\mu\text{m}$	Oil viscosity	0.032	Pa.s
Shaft radius ( $R$ )	25	mm	External load ( $W_a$ )	320	N
Shaft mass ( $M$ )	10	kg			

The parametric analysis is performed by keeping the chevron thickness ( $e$ ) constant and varying the values of the chevron angle ( $\alpha$ ) between  $30^\circ$  and  $70^\circ$ , and the number of chevrons ( $N_t$ ) between 0 and 15. One observes the effect of the texture in the resultant eccentricity of the shaft for the operating condition in the study:

$$\varepsilon = \frac{\sqrt{X^2 + Y^2}}{h_N} \tag{7}$$

The obtained results are shown in Fig. 3 for different values of chevron thickness ( $3 \leq e \leq 7 \text{ mm}$ ). As one can see, for every chevron thickness, there is an optimum combination of angle  $\alpha$  and number of chevrons  $N_t$  that decreases the shaft eccentricity (an evidence of an increase of the bearing load-carrying capacity). In this case, the best results were obtained for  $N_t = 7$ ,  $e = 7 \text{ mm}$ , and  $\alpha = 60^\circ$ . The resultant eccentricity was  $\varepsilon = 0.184$ , which is 9.4% smaller than that of the shaft without textures ( $\varepsilon = 0.203$ ) (Fig. 4).

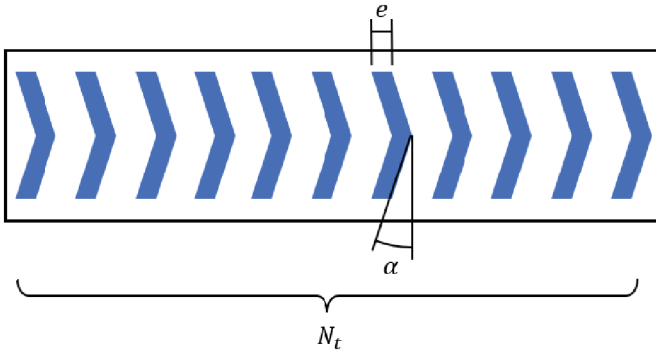


**Fig. 3.** Geometric parameters of the chevron texture on the shaft surface: chevron angle ( $\alpha$ ), chevron thickness ( $e$ ), and the number of chevrons ( $N_t$ ).

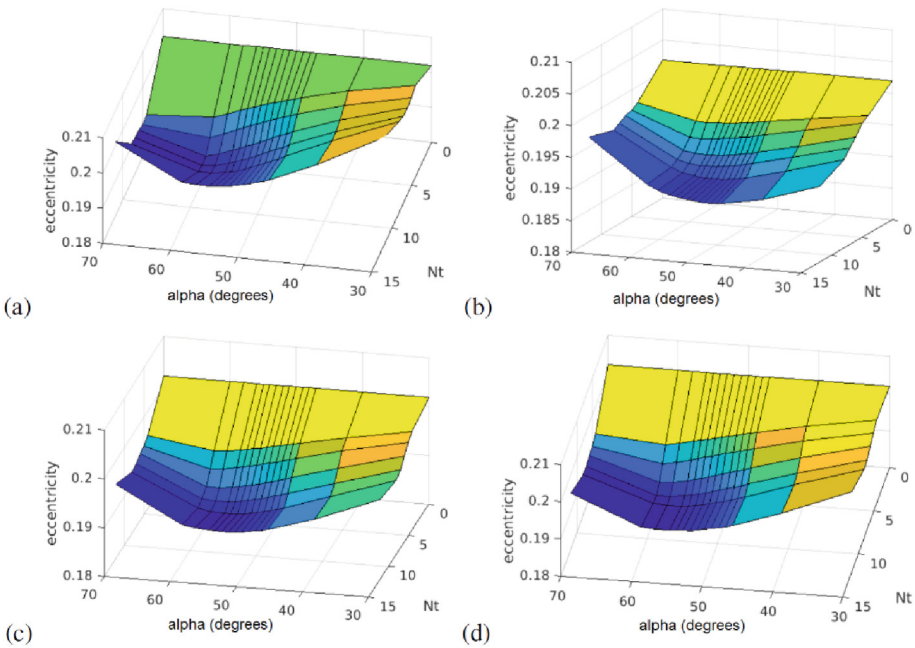


**Fig. 4.** Shaft eccentricity as a function of the texture angle  $\alpha$  and the number of textures  $N_t$ : (a)  $e = 3$  mm, (b)  $e = 4$  mm, (c)  $e = 5$  mm, (d)  $e = 7$  mm.

To better understand why the textured shaft leads to a smaller eccentricity, let's analyze the case of the shaft with the best texture obtained in the parametric analysis ( $N_t = 7, e = 7$  mm,  $\alpha = 60^\circ$ ). Figure 5 presents the hydrodynamic pressure distribution in the bearing gap, for a given instant of time, for the cases of non-textured and textured shafts. In the case of the non-textured shaft (Fig. 5a), one observes a conventional hill-shape distribution of the pressure around the position of minimum film thickness, with a maximum hydrodynamic pressure of  $5.9 \times 10^5$  Pa. This pressure distribution has a

convex shape in the direction of the shaft rotation, which tends to push the lubricant towards the axial boundaries of the bearing (leakage flow – Fig. 6a).

In the case of the textured shaft (Fig. 5b), the pressure distribution is completely different: the pressure distribution is concentrated in the regions between the chevrons because of the cavitation and pressure build-up zones created by them. For this reason, these pressure “hills” tend to follow the shape of the chevrons, thus presenting a concave shape in the direction of the rotating speed. As a consequence, the lubricant is not totally pushed toward the axial boundaries of the bearing. It is rather pushed towards the bearing centerline by the texture (Fig. 6b), in a clear *pumping effect* that keeps more lubricant in the bearing gap. As a result, more lubricant remains in the region of minimum film thickness, thus reducing the leakage flow, increasing the hydrodynamic pressure (maximum value of  $9.1 \times 10^5$  Pa) and, consequently, increasing the load-carrying capacity of the bearing.

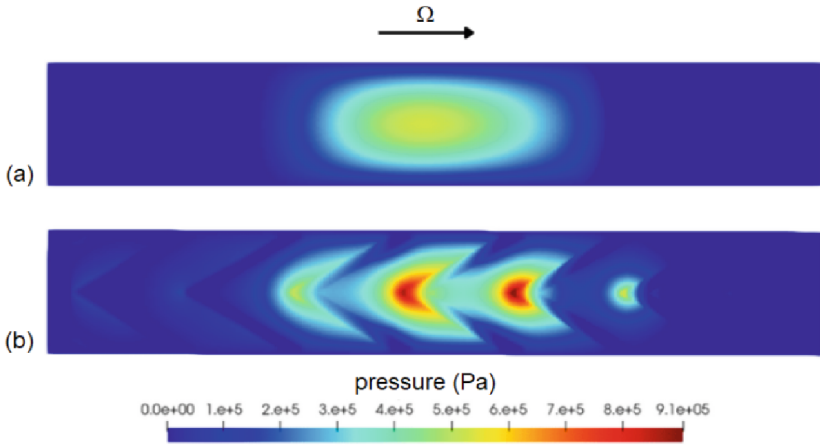


**Fig. 5.** Hydrodynamic pressure distribution at a given instant of time: (a) non-textured shaft, (b) chevron textured shaft ( $N_t = 7$ ,  $e = 7$  mm,  $\alpha = 60^\circ$ ).

This pumping effect is reversed if the shaft runs in the opposite direction. Figure 7 presents the hydrodynamic pressure and lubricant flow in the bearing gap for this situation. As one can see, the pressure distribution still concentrates in the regions between the chevron textures. However, due to the direction of the shaft surface motion, the pressure “hill” now has a convex shape which reverses the pumping effect. The lubricant is pushed towards the axial boundaries of the bearing, thus decreasing the volume of lubricant in the bearing gap and, consequently, increasing the leakage flow and reducing the hydrodynamic pressure. This reversed pumping effect increases the leakage flow in comparison to the non-textured case, thus resulting in a much higher shaft eccentricity ( $\varepsilon = 0.420$  – an increase of 107% in comparison to the non-textured case). Hence, the direction of shaft rotation and the orientation of the chevron textures on the shaft are important parameters that define the success or failure to increase the load-carrying capacity of the bearing.

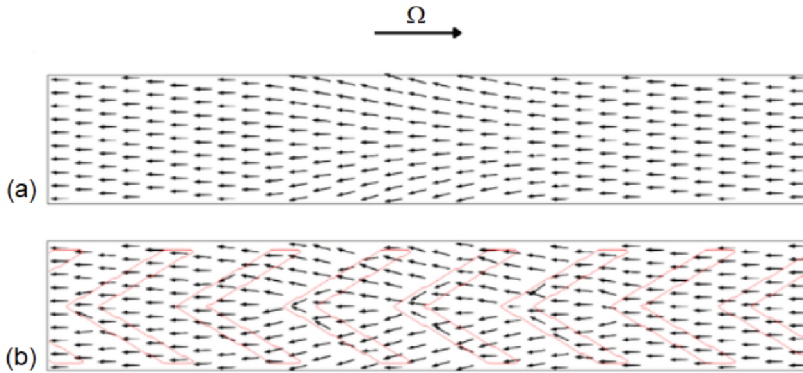


**Fig. 6.** Lubricant flow in the bearing gap: (a) non-textured shaft, (b) chevron textured shaft.

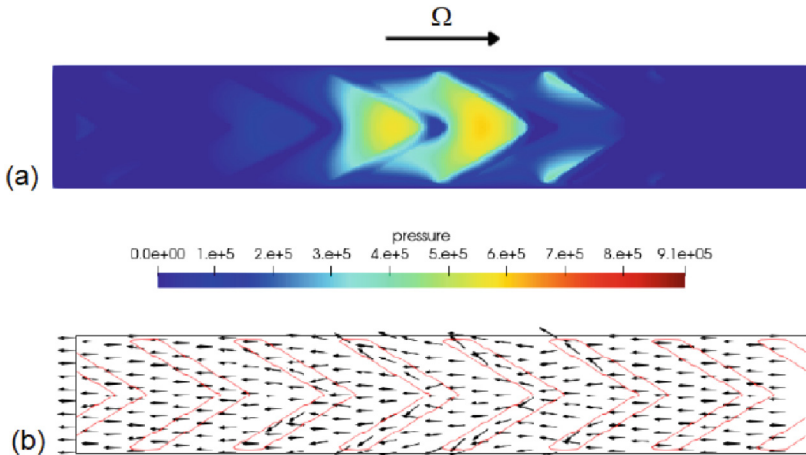


**Fig. 7.** Effect of running the shaft with chevron textures in the opposite direction: (a) hydrodynamic pressure distribution, (b) lubricant flow.

The above results clearly show that there are optimum values for the texture parameters ( $N_f$ ,  $e$ ,  $\alpha$ ) according to the bearing operating condition. Although the optimization of the chevron texture is beyond the scope of the present work, further investigations in this direction showed that:

- $N_f$  decreases for increasing Sommerfeld numbers;
- $e$  increases for increasing Sommerfeld numbers;
- $\alpha$  increases for increasing Sommerfeld numbers.

In all these cases, one achieved optimum load-carrying capacity with the optimum chevron geometry.



## 4 Conclusion

The parametric analysis of the chevron texture applied to the surface of the rotating shaft in journal bearings showed that the rotor eccentricity can be reduced in the textured cases, as evidence of the increase of bearing load-carrying capacity. Such an increase in the bearing load-carrying capacity is a consequence of the pumping effect that occurs in the lubricant flow caused by the cavitation and pressure build-up zones created by the textures as they run over the lubricant. For this reason, the direction of shaft rotation and the orientation of the chevron textures on the shaft play important roles in the supporting mechanism of the journal bearing: the convex side of the chevron texture must be in the direction of motion of the shaft surface. Optimum texture geometries can be found for the given operating conditions of the bearing.

**Acknowledgements.** This project was supported by the Brazilian research foundations Conselho Nacional de Desenvolvimento Científico e Tecnológico (Grant no.: 304212/2021-0) and Fundação de Amparo à Pesquisa do Estado de São Paulo (Grant no.: 2021/00327-6).

## References

1. Anno, J.N., Walowit, J., Allen, C.: Microasperity lubrication. *J. Lubr. Technol.* **90**(2), 351–355 (1968)
2. Hamilton, D., Walowit, J., Allen, C.: A theory of lubrication by microirregularities. *J. Basic Eng.* **88**(1), 177–185 (1966)
3. Wang, X., Kato, K., Adashi, K., Aizawa, K.: Loads carrying capacity map for the surface texture design of SiC thrust bearing sliding in water. *Tribol. Int.* **36**(3), 189–197 (2003)
4. Wakuda, M., Yamauchi, Y., Kanzaki, S., Yasuda, Y.: Effect of surface texturing on friction reduction between ceramic and steel materials under lubricated sliding contact. *Wear* **254**(3–4), 356–363 (2003)
5. Etsion, I., Halperin, G., Brizmer, V., Kligerman, Y.: Experimental investigation of laser surface textured parallel thrust bearings. *Tribol. Lett.* **17**(2), 295–300 (2004)
6. Hao, X., Sun, H., Wang, L., Ali, Q., Li, L., He, N.: Fabrication of micro-texture on cylindrical inner surface and its effect on the stability of hybrid bearing. *Int. J. Adv. Manuf. Technol.* **109**(5–6), 1671–1680 (2020). <https://doi.org/10.1007/s00170-020-05750-8>
7. Costa, H., Hutchings, I.: Effects of die surface patterning on lubrication in strip drawing. *J. Mater. Process. Technol.* **209**(3), 1175–1180 (2009)
8. Silva, E.J., Kirsch, B., Bottene, A.C., Simon, A., Aurich, J.C., Oliveira, J.F.G.: Manufacturing of structured surfaces via grinding. *J. Mater. Process. Technol.* **243**, 170–183 (2017)
9. Shen, C., Khonsari, M.: Texture shape optimization for seal-like parallel surfaces: theory and experiment. *Tribol. Trans.* **59**(4), 698–706 (2016)
10. Galda, L., Sep, J., Olszewski, A., Zochowski, T.: Experimental investigation into surface texture effect on journal bearings performance. *Tribol. Int.* **136**, 372–384 (2019)
11. Yue, H., Deng, J., Ge, D., Li, X., Zhang, Y.: Effect of surface texturing on tribological performance of sliding guideway under boundary lubrication. *J. Manuf. Process.* **47**, 172–182 (2019)
12. Gropper, D., Wang, L., Harvey, T.J.: Hydrodynamic lubrication of textured surfaces: a review of modeling techniques and key findings. *Tribol. Int.* **94**, 509–529 (2016)

13. Sharma, S., Jamwal, G., Awasthi, R.K.: Enhancement of steady state performance of hydrodynamic journal bearing using chevron-shaped surface texture. *J. Eng. Tribol.* **233**(12), 1833–1843 (2019)
14. Liang, X., Liu, Z., Wang, H., Zhou, X., Zhou, X.: Hydrodynamic lubrication of partial textured sliding journal bearing based on three-dimensional CFD. *Ind. Lubr. Tribol.* **68**(1), 106–115 (2016)
15. Shen, C., Khonsari, M.: Effect of dimple's internal structure on hydrodynamic lubrication. *Tribol. Lett.* **52**(3), 415–430 (2013)
16. Papadopoulos, C., Kaiktsis, L., Fillon, M.: Computational fluid dynamics thermohydrodynamic analysis of three-dimensional sector-pad thrust bearings with rectangular dimples. *J. Tribol.* **136**(1), 011702 (2014)
17. Manser, B., Belaidi, I., Hamrani, A., Khelladi, S., Bakir, F.: Texture shape effects on hydrodynamic journal bearing performances using mass-conserving numerical approach. *Tribol. Mater. Surf. Interfaces* **14**(1), 33–50 (2020)
18. Jamwal, G., Sharma, S., Awasthi, R.: The dynamic performance analysis of chevron shape textured hydrodynamic bearings. *Ind. Lubr. Tribol.* **72**, 1–8 (2019)
19. Yin, B., Li, X., Fu, Y., Yun, W.: Effect of laser textured dimples on the lubrication performance of cylinder liner in diesel engine. *Lubr. Sci.* **24**(7), 293–312 (2012)
20. Tanaka, H., Ichimaru, K.: Numerical simulation of oil-film behavior on cylinder liners in sliding contacts with piston rings. *Tribol. Ser.* **43**, 283–290 (2003)
21. Filgueira Filho, I.C.M., Bottene, A.C., Silva, E.J., Nicoletti, R.: Static behavior of plain journal bearings with textured journal experimental analysis. *Tribol. Int.* **159**, 106970 (2021). <https://doi.org/10.1016/j.triboint.2021.106970>
22. Sinanoglu, C.: The analysis of the effects of surface texture on the capability of load carriage of journal bearings using neural network. *Ind. Lubr. Tribol.* **57**(28–40), 293–312 (2005)
23. Gerya, T.: *Introduction to Numerical Geodynamic Modelling*. Cambridge University Press (2019). <https://doi.org/10.1017/9781316534243>